Shear-induced crystallization in jammed systems

Nathan Duff and Daniel J. Lacks
Department of Chemical Engineering, Case Western Reserve University, Cleveland, Ohio 44106, USA
(Received 6 September 2006; revised manuscript received 17 November 2006; published 16 March 2007)

Simulations are used to address the effects of oscillating shear strain on jammed systems composed of spherical particles. The simulations show that shear oscillations with amplitudes of more than a few percent lead to substantial crystallization of the system. To ensure that the conclusions are independent of the simulation methodology, a range of simulations are carried out that use both molecular dynamics and athermal dynamics methods, soft and hard potentials, potentials with and without attractive forces, and systems with and without surrounding walls. The extent of crystallization is monitored primarily by the Q_6 order parameter, but also in some simulations by the potential energy and the radial distribution function, and by direct visual inspection. A mechanism is proposed for shear-induced crystallization of jammed systems, based on fold catastrophes of the free-energy landscape.

DOI: 10.1103/PhysRevE.75.031501 PACS number(s): 83.10.Rs, 61.43.Fs, 61.20.Ja, 62.20.Fe

I. INTRODUCTION

Upon fast cooling, a liquid can become kinetically trapped in a glassy state characterized by structural disorder and the absence of diffusive dynamics. The glassy state can persist for very long times, even though a crystalline state is the thermodynamically stable state at low temperature. Recent work suggests a generality of this phenomenology [1], in that a broad range of systems can be trapped in "jammed" states characterized by structural disorder and the absence of diffusive dynamics. In this general picture, diffusive dynamics are controlled not only by temperature, but also by density and applied driving force. For some systems, such as molecular systems and colloids, all three of these factors affect dynamics; in other systems, such as granular materials, thermal fluctuations are negligible, and only the density and applied driving force are relevant.

The present investigation addresses the role of driving force in moving *jammed* disordered systems to crystalline states. This analysis is relevant to all jammed systems that can crystallize, including molecular-level glasses, monodisperse colloidal glasses, and granular materials consisting of spherical particles. The focus of this work is distinct from work that addressed shear-induced structural changes in unjammed (liquidlike) systems, both experimentally in colloids [2–5] as well as with molecular [6,7], Brownian [8,9], and Stokesian [10] dynamics simulations.

In jammed systems, experiments have shown that a driving force can induce crystallization in systems that would otherwise remain disordered. Vibrations [11–14], shear oscillations [15–17], and steady shear [18,19] have been used to induce crystallization in granular materials of spherical particles. Similarly, shear oscillations have been used to induce crystallization in colloidal glasses [20].

The shear-induced crystallization in jammed systems has not been addressed with simulations, which rather have focused on unjammed systems. The physics that underlie shear-induced structural changes are fundamentally different in jammed and unjammed systems—in jammed systems, shear provides the only means for diffusive dynamics that allow the particles to rearrange to a different structure, while in unjammed systems the particles already undergo the diffusive dynamics necessary for restructuring.

II. COMPUTATIONAL METHODS

Simulations are carried out to determine the effects of shear oscillations on the extent of crystallization in athermal and glassy systems composed of spherical particles. The extent of crystallization is monitored several ways: a bond-order parameter, the radial distribution function, the potential energy, and direct visual inspection.

The bond-order parameter Q_6 has been widely used to quantify crystallization in spherical particle systems [21]. This parameter is defined as

$$Q_6 = \left[\left(\frac{4\pi}{13} \right) \sum_{m=-6}^{6} |\langle Y_{6m} \rangle|^2 \right]^{1/2},$$

where $\langle Y_{6m} \rangle$ is the average value of the spherical harmonic for the N_{bonds} "bonds" in the system (a "bond" is defined here as a particle separated by a distance less than 1.3 times the particle diameter). For disordered structures, the value of Q_6 is small; $Q_6 \approx 1/\sqrt{N_{bonds}}$ for fully disordered systems [22]. The value of Q_6 is significantly larger for ordered systems; e.g., $Q_6=0.5745$ for an fcc crystal, $Q_6=0.5106$ for a bcc crystal, and $Q_6=0.6633$ for an icosahedron [22].

The simulations begin from initially disordered configurations (with some exceptions described below). These initial configurations are prepared by using molecular-dynamics simulations to quench liquid systems to glasslike states. In continuous-potential systems the quenching is carried out by rapidly decreasing the temperature, and in discontinuous-potential systems the quenching is carried out by rapidly decreasing the volume. Additionally, some simulations begin from a perfect fcc structure.

Several types of simulations are carried out to ensure that the conclusions are independent of the type of system and simulation methodology. In particular, the simulations address both continuous ("soft") and discontinuous ("hard") potential systems: systems that are purely repulsive and systems that include attractive interactions; and systems that

have periodic boundary conditions and systems that are surrounded by walls. The particle dynamics is modeled by both finite temperature molecular dynamics, and an athermal dynamics algorithm that includes no thermal effects.

A. Repulsive soft-spheres, periodic boundary conditions, and athermal dynamics

In these simulations, the particles are repulsive soft spheres described by the truncated and shifted Lennard-Jones potential,

$$U(r_{ij}) = 4\varepsilon\left[\left(\frac{r_{ij}}{\sigma}\right)^{12} - \left(\frac{r_{ij}}{\sigma}\right)^{6}\right] - 4\varepsilon\left[\left(\frac{r_c}{\sigma}\right)^{12} - \left(\frac{r_c}{\sigma}\right)^{6}\right],$$

$$r_{ij} \leqslant r_c, \tag{1a}$$

$$U(r_{ij}) = 0, \quad r_{ij} > r_c, \tag{1b}$$

with $r_c = 2^{1/6}\sigma$. An orthogonal simulation cell with simulation cell lengths a_1, a_2, and a_3 is used, along with periodic boundary conditions. Pure shear strain is imposed in the simulations by changing the lengths of the sides of the simulation cell as follows:

$$a_1(t) = a_{1,0}[1 + A\,\sin(2\pi t/\tau_{osc})],$$

$$a_2(t) = a_{2,0}\left[\frac{1}{1 + A\,\sin(2\pi t/\tau_{osc})}\right], \quad a_3(t) = a_{3,0}, \tag{2}$$

where A and τ_{osc} determine the amplitude and frequency of the strain oscillations. The particle trajectories are determined by an athermal dynamics method [23],

$$m\frac{d^2x_{\alpha,i}}{dt^2} = F_{\alpha,i} - b\sum_j (v_{\alpha,i} - v_{\alpha,j}), \tag{3}$$

where the $x_{\alpha,i}$, $v_{\alpha,i}$, and $F_{\alpha,i}$ represent the position, velocity, and force, respectively, along the α coordinate for particle i, and b is a friction coefficient; the sum over j in the friction contribution involves only particles that are in contact with particle i (e.g., $r_{ij} < r_c$).

The athermal dynamics method describes the dynamics of granular materials, where each particle is macroscopic, and thus thermal fluctuations of the particle positions are negligible. Physically, the energy dissipated by friction in Eq. (3) would be associated with the atomic degrees of freedom within the particles, which are ignored at this level of simulation.

B. Lennard-Jones particles, periodic boundary conditions, and molecular dynamics

These simulations address particles described by a Lennard-Jones model, which is obtained from Eq. (1) with $r_c = 1.5\sigma$. The boundary conditions and imposition of shear strain are the same as in the simulations described above (Sec. A). The particle trajectories are determined by molecular dynamics with the Nosé-Hoover thermostat [24],

$$m\frac{d^2x_{\alpha,i}}{dt^2} = F_{\alpha,i} - qv_{\alpha,i}, \quad \frac{dq}{dt} = \frac{\sum_i mv_i^2 - 3(N-1)kT}{Q}, \tag{4}$$

where q is the extended system variable used to maintain constant temperature, and Q is the constant that controls the relaxation time for q. The simulations are carried out with $Q = 2.41\sigma^2$.

C. Hard spheres, hard walls, and event-driven dynamics

These simulations address hard-sphere particles in a box surrounded by hard walls. The particle trajectories are obtained with an event-driven method for hard-particle dynamics [24]. Since trajectories in event-driven methods are most easily determined when all components move at constant velocity between collisions, strain is imposed by moving the positions of the walls at constant velocity,

$$a_1(t) = a_{1,0}[1 + v_{wall}t], \quad a_2(t) = a_{2,0}[1 - v_{wall}t], \quad a_3(t) = a_{3,0}, \tag{5}$$

where v_{wall} is the wall velocity. Note that the volume is not constant under this protocol; however, the volume changes are small for small strains, and such that the volume is always less than the initial volume. To impose oscillation of the wall positions, the sign of v_{wall} is switched periodically. Since energy is continuously put into the system via the moving walls, the velocities are rescaled after each collision so that the energy of the system (i.e., mean-squared velocity of particles, $\langle v^2 \rangle$) remains constant; this rescaling acts to change the time scale of the simulation, and is necessary in order to compare the rates of crystallization for the sheared and unsheared systems. The spheres are of diameter σ, and the characteristic time τ is defined as $\tau = \sigma^2/\langle v^2 \rangle$.

III. RESULTS

A. Repulsive soft spheres, periodic boundary conditions, and athermal dynamics

Results are shown in Fig. 1 for a system of 4000 particles at density $\rho = 2^{1/2}\sigma^{-3}$, with a friction coefficient $b = 0.04$ $(\varepsilon m\sigma^{-2})^{1/2}$, going through ten cycles of shear with strain amplitude $A = 0.05$. The results for Q_6 show the evolution of the extent of crystallization in the system, and are compared to results in the absence of strain oscillations. The system begins in a disordered state, as characterized by the initially small value of $Q_6 \sim 0.01$. The value of Q_6 increases slightly during the first shear oscillation, and then increases significantly to $Q_6 \sim 0.4$ during the second shear oscillation; in comparison, Q_6 remains low throughout the simulation when the system is not strained. Thus two strain oscillations induce significant crystallization in this system (note Q_6 is less than the value for an fcc crystal due to the crystal structure being imperfect). For further shear oscillations, the value of Q_6 fluctuates about $Q_6 \sim 0.4$, with a standard deviation of ~ 0.05; these fluctuations occur because shear acts to repeatedly induce and destroy order. The mean-squared displacements of the particles, shown in Fig. 1(c), increase mono-

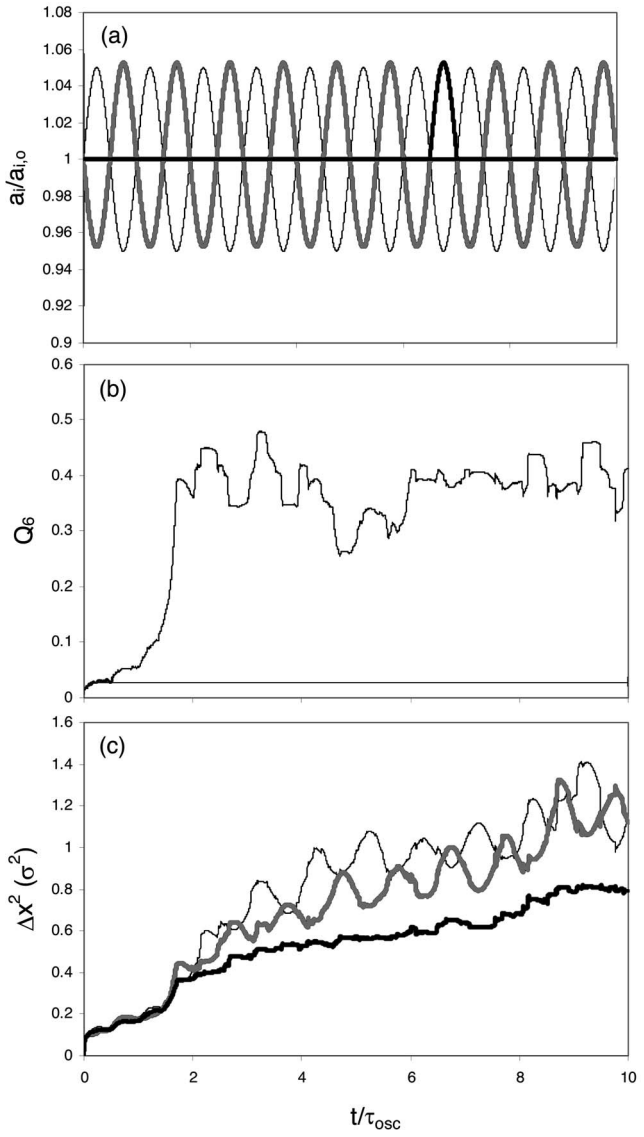

FIG. 1. Results for system of 4000 soft-sphere particles undergoing athermal dynamics with strain amplitude $A=0.05$. (a) Time dependence of the strains along the x, y, and z directions. (b) Order parameter Q_6 (thick line), compared with the result in the absence of strain oscillation (thin line). (c) Mean-squared displacements, along the x, y, and z directions; parts (a) and (c) use the same line symbols to denote results along the x, y, and z directions.

tonically with time when the system is disordered (e.g., first two strain cycles), but undergo large oscillations in the directions undergoing strain oscillations when the system is ordered.

Results for simulations with various strain amplitudes, ranging from $A=0.05$ to 0.50, are shown in Fig. 2. Crystallization occurs more quickly when the shear oscillates with larger amplitudes. All of these systems appear to reach a similar steady state, characterized by $Q_6 \sim 0.4$, regardless of the strain amplitude. For the simulations with $A=0.25$ and 0.50, the mean-squared displacement vs time results are characterized by a slope of approximately 1 on a log-log plot, which implies that the particles undergo strain-induced diffusive dynamics. This diffusion occurs even after the system becomes highly crystalline, and can be understood in terms of the repeated strain-induced formation and destruction of order in the system that accompanies the fluctuations in Q_6 (as discussed above).

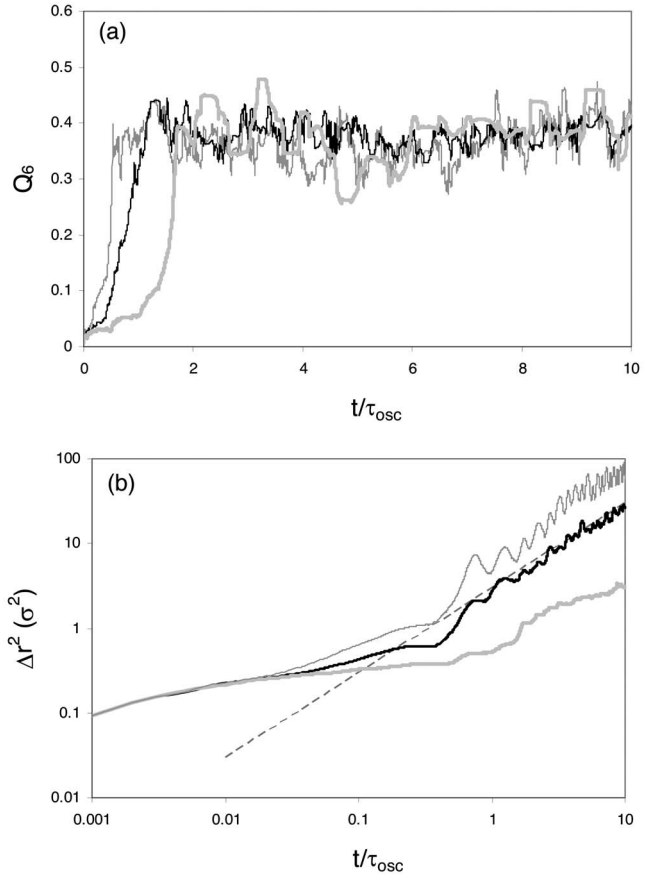

FIG. 2. Comparison of results for simulations with various strain amplitudes. All results are for systems of 4000 soft-sphere particles undergoing athermal dynamics. (a) Order parameter Q_6. (b) Mean-squared displacements. Results are for $A=0.05$ (thick gray line), $A=0.25$ (black line), and $A=0.50$ (thin gray line). The dashed line in part (b) shows a slope of 1 on the log-log plot.

Simulations are also carried out that begin from a perfect fcc crystal, and the Q_6 results for these simulations are shown in Fig. 3. The fcc crystal is stable with respect to shear oscillations for shear strains $(a_1/a_{1,0}-1)<0.088$. However, larger shear strains partially destroy the crystalline order, and the shear oscillations move the system to a steady state that is apparently the same partially crystalline state obtained when an initially disordered state is sheared.

To assess the generality of these results, simulations on this system were carried out with system sizes ranging from 108 to 32 000 particles, various values of the friction coefficient b, various oscillation periods τ_{osc}, and other combinations of shear strain. The results are similar in all cases. As an example, Fig. 4 shows results for a 32 000-particle system with strain imposed in three dimensions as

$$a_1(t) = a_{1,0}[1 + A_1 \sin(2\pi t/\tau_{osc,1})],$$

$$a_2(t) = a_{2,0}[1 + A_2 \sin(2\pi t/\tau_{osc,2})],$$

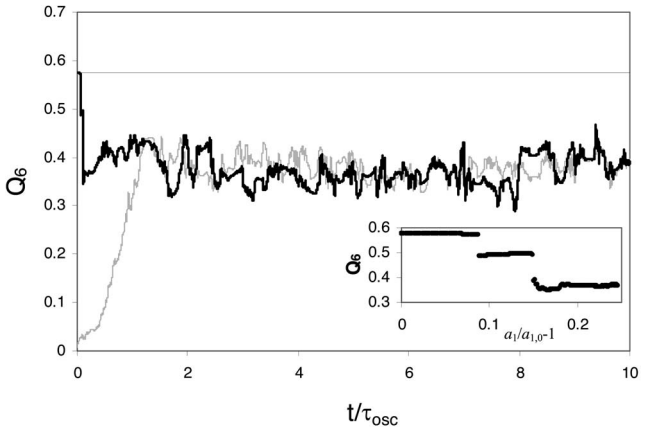

FIG. 3. Results for Q_6 for simulations starting from a perfect fcc crystal. The thick black line represents results for $A=0.25$, and the thin black line represents results for $A=0.05$ (note that for $A=0.05$, Q_6 is always approximately 0.57). For comparison, the gray line represents results for $A=0.25$ starting from a disordered configuration. Inset: Closeup of results for $A=0.25$ plotted as a function of strain rather than time.

$$a_3(t) = a_{3,0}\left[\frac{1}{1+A_1\sin(2\pi t/\tau_{osc,1})}\right]\left[\frac{1}{1+A_2\sin(2\pi t/\tau_{osc,2})}\right]. \tag{6}$$

The results for this 32 000-particle simulation are similar to the results for the smaller simulations described above. However, a greater number of shear oscillations are required to induce order in this larger system. A snapshot of a particle configuration from the latter part of this simulation is shown in Fig. 5, and compared to the initial disordered configuration. The view is along the [111] direction of the crystal; when a perfect fcc crystal is viewed from this direction, particles are lined up such that only the top particle is visible. This snapshot corroborates the conclusion based on the values of Q_6, that the system has become highly crystalline.

B. Lennard-Jones particles, periodic boundary conditions, and molecular dynamics

Results are shown in Fig. 6 for the Lennard-Jones system with the trajectory determined by molecular-dynamics simulation at finite (but low) temperature. The simulations are carried out at $T=0.01\ \varepsilon/\mathrm{k}$, for a 4000-particle system at density $\rho=1\sigma^{-3}$. Results are shown for simulations with oscillating strains (with $A=0.05$ and 0.25), as well as in the absence of strain. The results for Q_6 indicate shear-induced crystallization that is similar to that obtained for the soft-sphere system with athermal dynamics. Thus, the presence of attraction in the potential or thermal dynamics (at low temperature) does not alter the nature of the shear-induced crystallization process. Also, the similarity of the molecular-dynamics and athermal-dynamics results suggest that the results are independent of the type of thermostat used in the molecular-dynamics simulation. The reason why the results are independent of the choice of thermostat is that the systems are examined near the low-temperature and low-shear rate limit, where the system would closely follow a quasistatic trajectory (i.e., the system remains near a local energy minimum at all times) regardless of the type of thermostat.

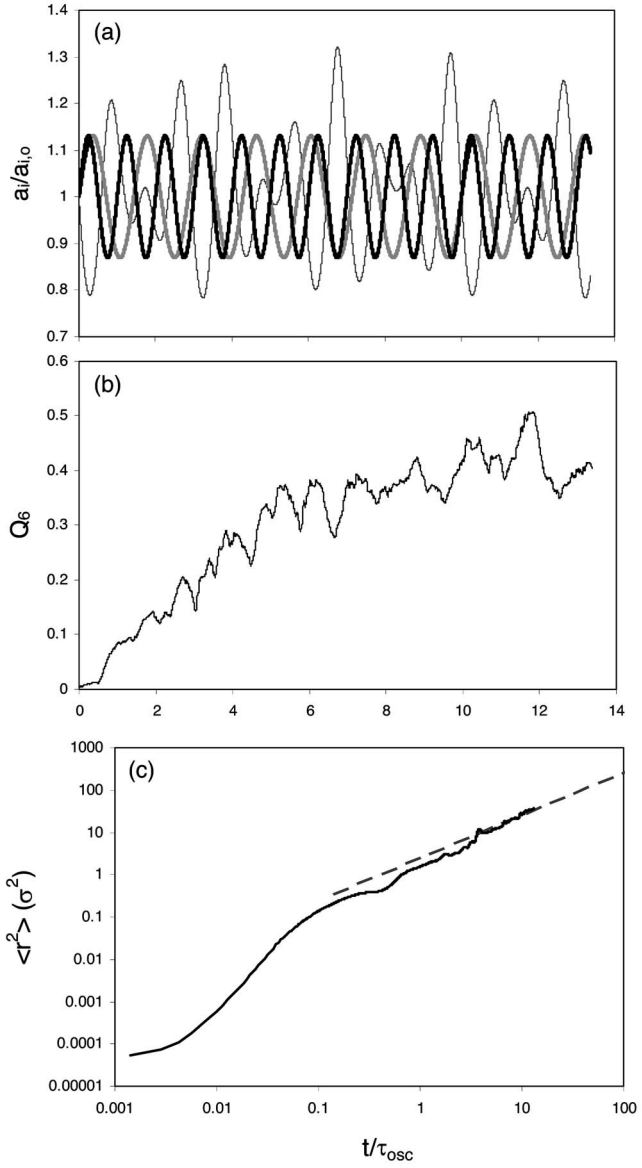

FIG. 4. Results for a system of 32 000 soft-sphere particles undergoing athermal dynamics. (a) Time dependence of the strains along the x, y, and z directions. (b) Order parameter Q_6. (c) Mean-squared displacements. The dashed line in part (b) shows a slope of 1 on the log-log plot.

Also shown in Fig. 6 are results for the potential energy per particle. The energy is normalized by ε', where ε' is the well depth of the truncated potential, $\varepsilon'=\varepsilon[1-(r_c/\sigma)^{12}+(r_c/\sigma)^6]$. For the Lennard-Jones system, the potential energy serves as an additional order parameter in regard to crystallization—i.e., for an fcc crystal at $\rho=1\sigma^{-3}$, $E/\varepsilon'=-6$, and E/ε' is higher (i.e., less negative) for disordered systems (note that the potential is truncated between the first and second coordination shells). The results in Fig. 6 show that the changes in the potential energy track

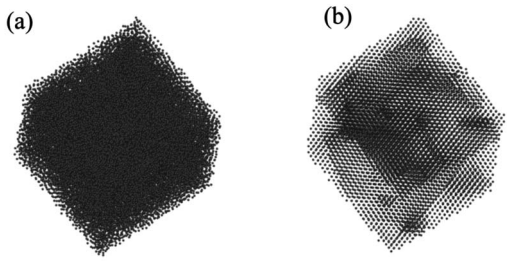

FIG. 5. Snapshots of configurations in the simulation with 32 000 particles and athermal dynamics. The view is along the [111] direction of the crystal; when a perfect fcc crystal is viewed from this direction, particles are lined up such that only the top particle is visible. (a) Initial disordered system; (b) same system after being subjected to shear oscillations. Note that the sphere sizes are not to scale, but are reduced in size for clarity.

the changes in Q_6, and support the conclusion that shear strain induces significant crystallization.

The extent of crystallization was also examined in terms of the radial distribution function $g(r)$, and these results are shown in Fig. 7. The initial structure is described by a $g(r)$ that is characteristic of disordered condensed-phase systems. In contrast, the structure obtained after shear cycling is described by a $g(r)$ that has sharp peaks; these peaks occur at

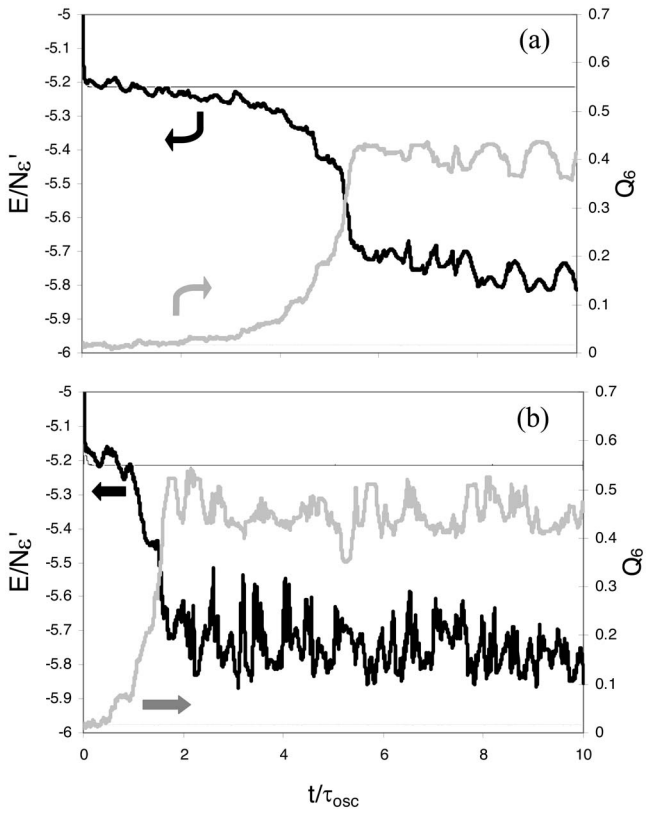

FIG. 6. Results for Q_6 and the potential energy for systems with 4000 Lennard-Jones particles undergoing Nosé-Hoover dynamics. (a) Results for $A=0.05$. (b) Results for $A=0.25$. Thick lines represent results for systems subjected to strain oscillations, and thin lines represent results in the absence of strain (for comparison).

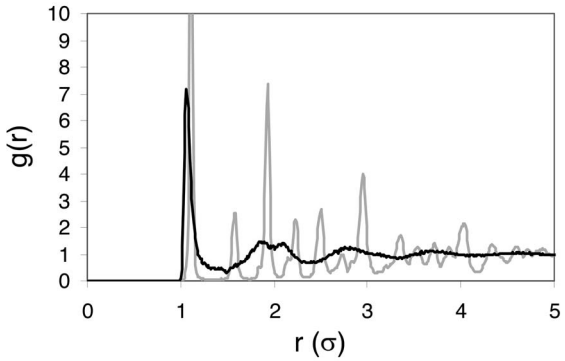

FIG. 7. Results for the radial distribution function $g(r)$ for a system with 4000 Lennard-Jones particles undergoing Nosé-Hoover dynamics. The black line represents $g(r)$ for the initial structure, and the gray line represents $g(r)$ after ten shear cycles.

distances of $n^{1/2}2^{1/6}\sigma(n=1,2,3,\ldots)$, indicative of an fcc crystal at $\rho=1\sigma^{-3}$. These results again corroborate the conclusion that shear produces an fcc crystalline structure from initially disordered structures.

C. Hard spheres, hard walls, and event-driven dynamics

Figure 8 shows results for a hard-sphere system undergoing athermal dynamics. The simulations of hard-sphere systems are carried out with 864 particles at packing fractions $\phi=0.55$ and 0.57. The simulations are carried out at packing fractions below the jamming transition (in the supercooled liquid regime); a jammed hard-sphere system could not be simulated because the particle collision frequency diverges as the system becomes jammed. Thus these hard-sphere systems will crystallize to some extent during the time scales of the simulation, even in the absence of strain oscillations. The simulations begin from disordered states with $Q_6 \sim 0.07$, and are run for times of 500τ (corresponding to 10^7-10^8 collisions). In the *absence* of strain oscillations, Q_6 reaches ~ 0.29 in the simulation with $\phi=0.55$, and Q_6 reaches ~ 0.17 in the simulation with $\phi=0.57$.

Results are also shown in Fig. 8 for systems under oscillating shear strain, with wall velocities $v_{wall}=0.05\sigma/\tau$. The strain oscillations enhance the rates of crystallization in both the $\phi=0.55$ and 0.57 systems, in comparison to the results with no strain oscillation. In all cases, strain oscillations lead to crystallization such that Q_6 reaches steady states in the range of 0.4–0.5. Simulations were also carried out at other wall velocities; similar behavior occurs for all wall velocities investigated, including wall velocities up to $v_{wall}=10\,000\sigma/\tau$.

We note that previous studies addressed hard-sphere systems with vibrating walls, but at much lower packing fractions where the system is gaslike rather than jammed [25–27].

IV. DISCUSSION

A. Physical basis of shear-induced crystallization in jammed systems

At equilibrium, the average depth of the energy minima visited by a disordered system is a well-defined property that

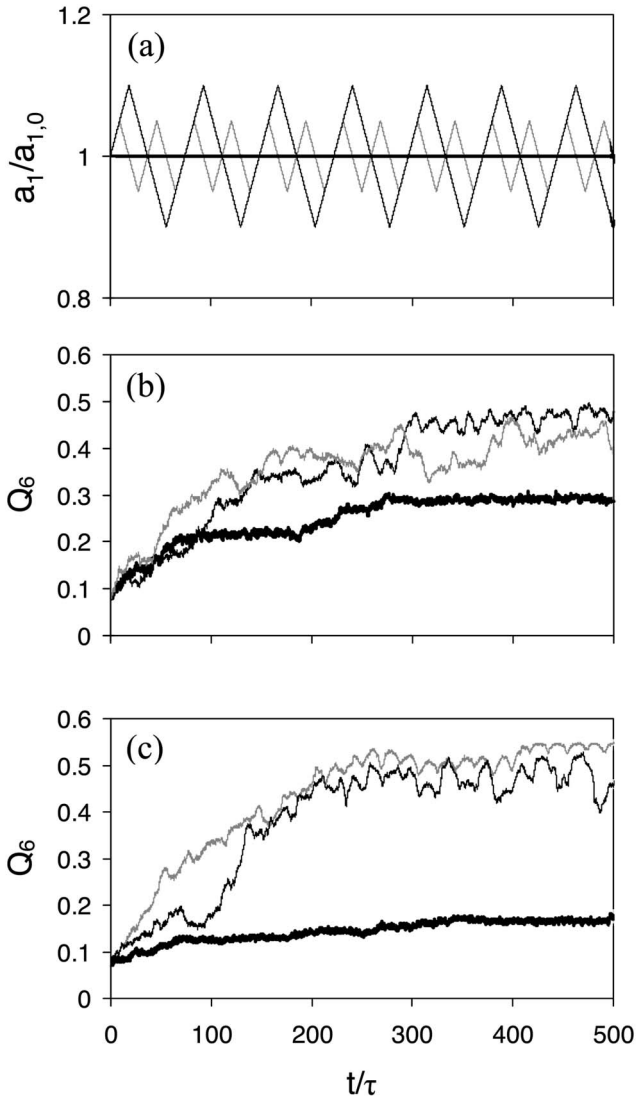

FIG. 8. Results for hard-potential systems. (a) Strain along one dimension as a function of time; note that strain along one other dimension is equal and opposite to this strain, and there is no strain along the third dimension. (b) Results for Q_6 as a function of time, at a packing fraction $\phi=0.55$. (c) Results for Q_6 as a function of time, at a packing fraction $\phi=0.57$. In all parts, the thick black line represents results in the absence of strain, the gray line represents results for a strain amplitude of 5%, and the thin black line represents results for a strain amplitude of 10%.

increases with decreasing temperature [28]. After rapid cooling, the system moves with time over the energy landscape to the deeper energy minima that characterize equilibrium at the new temperature [29]. If this rapid cooling brings the system into a glassy state, the dynamics by which the system moves towards the deeper energy minima become very slow. These slow dynamics in glasses, by which the system moves to deeper energy minima, are called aging processes.

Experiments on polymer and colloidal systems show that mechanical deformation can effectively reverse [30–37] or accelerate [38–41] aging, depending on the situation. These experimental results are elucidated by molecular simulations

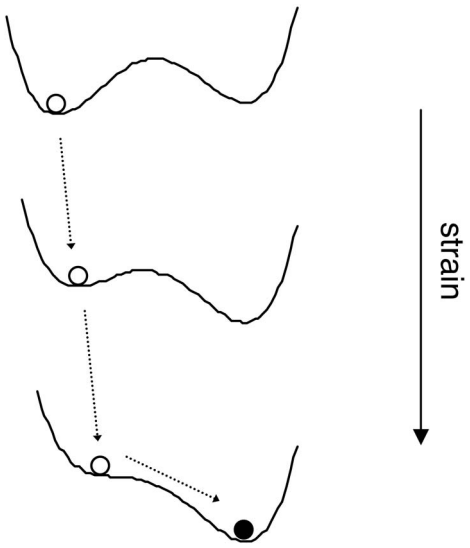

FIG. 9. Schematic representation of the strain-induced changes of the energy landscape that lead to a fold catastrophe. The circles represent the state of the system, and show how it changes due to the fold catastrophe.

on systems that cannot crystallize, which show that cycles of large strain move the system to shallower energy minima and effectively reverse aging, while cycles of small strain move the system to deeper energy minima and effectively accelerate aging [42,43].

In *jammed* systems, shear-induced crystallization is a special case of accelerated aging by mechanical deformation—in both cases, mechanical deformation acts to move a jammed system to deeper energy minima. For systems composed of spherically symmetric particles, the deepest energy minima are associated with crystal structures, and thus crystallization is the end point of the aging process in these systems. Therefore, the same physical mechanism underlies shear-induced aging and shear-induced crystallization in jammed systems. Note that this statement only applies to shear-induced crystallization in *jammed* systems, and may not be relevant to shear-induced crystallization in unjammed (liquid) systems.

Interestingly, large strains do not fully reverse aging once the jammed system becomes partially crystalline, as they do for systems that are disordered [42]. Apparently, shear strain cannot force the system out of the region of the energy landscape corresponding to partially crystalline structures.

A driving force generates diffusive dynamics in jammed systems by lowering energy barriers to structural rearrangements, until the barriers ultimately disappear; after a barrier disappears, the system can undergo a structural rearrangement even in the absence of thermal energy [44,45]. The disappearance of an energy barrier is associated with a fold catastrophe of the energy landscape. Strain distorts the energy landscape and causes energy minima and saddle points to move in configuration space. A fold catastrophe, shown schematically in Fig. 9, occurs when an energy minimum and saddle point collide and annihilate each other. Strain-induced fold catastrophes have been shown to occur in soft

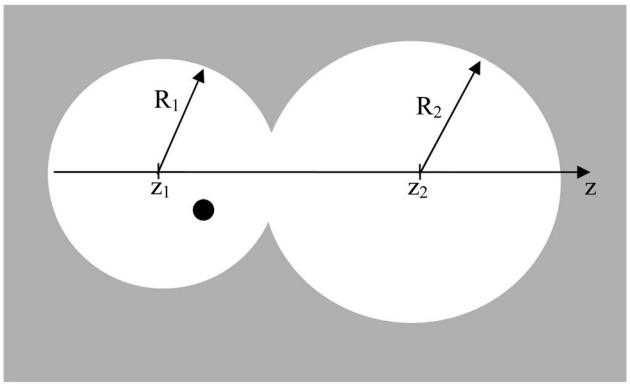

FIG. 10. Schematic of a simple model used to rationalize the mechanism of strain-accelerated dynamics in hard-potential systems.

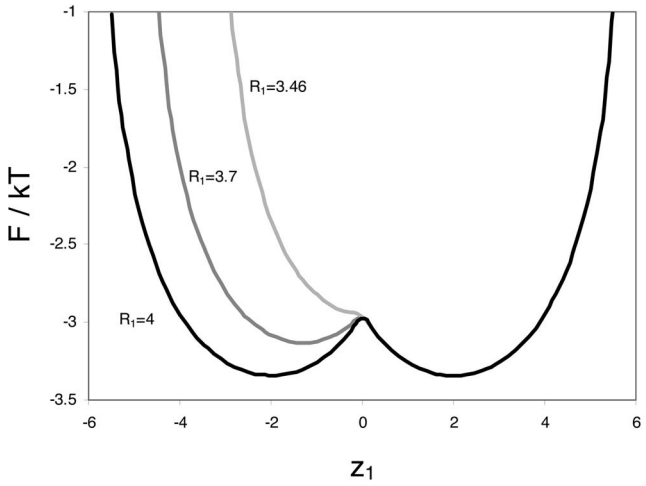

FIG. 11. Free-energy landscapes for the simple model shown in Fig. 10, as a function of the z coordinate of the particle.

particle systems through studies of the heights, positions, and curvatures of energy minima and saddle points of the energy landscape [46,47]. It is by this mechanism that shear cycles produce the structural rearrangements that ultimately move the system to crystalline energy minima.

B. Relationship of hard-potential and soft-potential results

The energy for a configuration of a hard potential system is either infinite or zero, depending on whether or not the particles overlap. Thus the energy landscape for a hard-sphere system will not include any minima or saddle points, and the energy landscape analysis discussed above is not relevant for hard-potential systems.

However, we suggest that fold catastrophes of the *free-energy* landscape underline shear-induced crystallization in hard-potential systems. In dense hard-particle systems, dynamics is limited by free-energy barriers with entropic origins. For example, a particle must escape the cage formed by neighboring particles in order to diffuse. To escape this cage, the particle may have to move through a narrow gap between two neighboring particles—the probability of moving through this gap via random motion may be small, thus leading to a free-energy barrier of entropic origin. Crystallization in the hard-potential system corresponds to the system moving to deeper *free-energy* minima, where the free-energy minima are separated by barriers with entropic origins. Strain can alter the rates of dynamical processes, and enhance crystallization, by distorting the free-energy landscape; for example, strain may act to decrease the size of the cage surrounding a particle, and thus destabilize the corresponding local free-energy minimum.

These effects are examined for a simple model, shown in Fig. 10, which represents a particle that can move between two cages. In this model, a hard-sphere particle is contained within a cavity bounded by hard walls, where the cavity is formed by two overlapping and truncated spheres; the diameter of the particle is σ, the radii of the spheres are R_1 and R_2, and the positions of the centers of the spheres along the z axis are z_1 and z_2. The partition function for the particle as a function of z is $q(z)=A_{\text{eff}}(z)$, where $A_{\text{eff}}(z)$ is the area of the cavity perpendicular to the z axis that is accessible to the particle. The free-energy landscape $F(z)$ is obtained from the partition function by $F(z)=-kT\ln q(z)$. The effect of strain can be incorporated in this model by changing the size and shape of the cavity via the values of R_1, R_2, z_1, and/or z_2.

Free-energy landscapes for this model are investigated with $\sigma=1$, $R_2=4$, $z_2=2$, and the values of R_1 and z_1 varied to mimic the effects of strain. Initially, $R_1=4$ and $z_1=-2$, and then R_1 is decreased while z_1 is changed such that $z_1=(R_1^2-R_2^2+z_2^2)^{1/2}$ (to maintain a constant hole diameter between cages). The free-energy landscapes are shown in Fig. 11—note that strain causes fold catastrophes in the free-energy landscape of this hard-potential system that are similar to the fold catastrophes in potential-energy landscapes of soft-potential systems.

Thus, we suggest that the shear-induced crystallization in the hard-sphere system is caused by fold catastrophes of the free-energy landscape. Fold catastrophes of the free-energy landscape are also relevant for the soft-potential systems; however, at low temperature the free energy is dominated by the potential energy, and so the free-energy fold catastrophes will nearly correspond to potential-energy fold catastrophes.

C. System size dependence of the results

Our results suggest that more shear oscillations are required to induce order for larger systems. For granular systems, the number of particles in our simulations is roughly comparable to the number of particles in experiments on granular systems, and thus the conclusions are directly applicable. However, for atomic glasses the number of particles is much larger than simulated here; thus, care must be taken in applying the present conclusions directly to atomic glasses.

ACKNOWLEDGMENT

This material is based upon work supported by the National Science Foundation under Grant No. DMR-0402867.

[1] A. J. Liu and S. R. Nagel, Nature (London) **396**, 21 (1998).
[2] B. J. Ackerson and P. N. Pusey, Phys. Rev. Lett. **61**, 1033 (1988).
[3] M. D. Haw, W. C. K. Poon, and P. N. Pusey, Phys. Rev. E **57**, 6859 (1998).
[4] R. M. Amos, J. G. Rarity, P. R. Tapster, T. J. Shepherd, and S. C. Kitson, Phys. Rev. E **61**, 2929 (2000).
[5] J. Vermant and M. J. Solomon, J. Phys.: Condens. Matter **17**, R187 (2005).
[6] J. Erpenbeck, Phys. Rev. Lett. **52**, 1333 (1984).
[7] H. Komatsugawa and S. Nose, Phys. Rev. E **53**, 2588 (1996).
[8] W. Xue and G. S. Grest, Phys. Rev. Lett. **64**, 419 (1990).
[9] S. Butler and P. Harrowell, J. Chem. Phys. **105**, 605 (1996).
[10] A. Sierou and J. F. Brady, J. Rheol. **46**, 1031 (2002).
[11] L. Vanel, A. D. Rosato, and R. N. Dave, Phys. Rev. Lett. **78**, 1255 (1997).
[12] O. Pouliquen, M. Nicolas, and P. D. Weidman, Phys. Rev. Lett. **79**, 3640 (1997).
[13] K. E. Daniels and R. P. Behringer, Phys. Rev. Lett. **94**, 168001 (2005).
[14] A. Cho, Science **311**, 1861 (2006).
[15] G. D. Scott, A. M. Charlesworth, and M. K. Mak, J. Chem. Phys. **40**, 611 (1964).
[16] M. Nicolas, P. Duru, and O. Pouliquen, Eur. Phys. J. E **3**, 309 (2000).
[17] N. W. Mueggenburg, Phys. Rev. E **71**, 031301 (2005).
[18] J.-C. Tsai, G. A. Voth, and J. P. Gollub, Phys. Rev. Lett. **91**, 064301 (2003).
[19] J. C. Tsai and J. P. Gollub, Phys. Rev. E **70**, 031303 (2004).
[20] M. D. Haw, W. C. K. Poon, P. N. Pusey, P. Hebraud, and F. Lequeux, Phys. Rev. E **58**, 4673 (1998).
[21] P. J. Steinhardt, D. R. Nelson, and M. Ronchetti, Phys. Rev. B **28**, 784 (1983).
[22] M. Rintoul and S. Torquato, J. Chem. Phys. **105**, 9258 (1996).
[23] N. Xu and C. S. O'Hern, Phys. Rev. Lett. **94**, 055701 (2005).
[24] M. P. Allen and D. J. Tildesley, *Computer Simulation of Liquids* (Clarendon, Oxford, 1989).
[25] S. McNamara and J.-L. Barrat, Phys. Rev. E **55**, 7767 (1997).
[26] P. E. Krouskop and J. Talbot, Phys. Rev. E **69**, 061308 (2004).
[27] O. Herbst, P. Muller, M. Otto, and A. Zippelius, Phys. Rev. E **70**, 051313 (2004).
[28] S. Sastry, P. G. Debenedetti, and F. H. Stillinger, Nature (London) **393**, 554 (1998).
[29] W. Kob, F. Sciortino, and P. Tartaglia, Europhys. Lett. **49**, 590 (2000).
[30] L. C. E. Struik, *Physical Aging in Amorphous Polymers and Other Materials* (Elsevier, Amsterdam, 1978).
[31] M. Cloitre, R. Borrega, and L. Leibler, Phys. Rev. Lett. **85**, 4819 (2000).
[32] V. Viasnoff and F. Lequeux, Phys. Rev. Lett. **89**, 065701 (2002).
[33] D. Bonn, S. Tanase, B. Abou, H. Tanaka, and J. Meunier, Phys. Rev. Lett. **89**, 015701 (2002).
[34] C. Derec, G. Ducouret, A. Ajdari, and F. Lequeux, Phys. Rev. E **67**, 061403 (2003).
[35] F. Ozon, T. Narita, A. Knaebel, G. Debregeas, P. Hebraud, and J.-P. Munch, Phys. Rev. E **68**, 032401 (2003).
[36] S. Kaloun, M. Skouri, A. Knaebel, J.-P. Munch, and P. Hebraud, Phys. Rev. E **72**, 011401 (2005).
[37] P. Busac, G. Lenormand, B. Fabry, M. Oliver, D. A. Weitz, V. Viasnoff, J. P. Butler, and J. J. Fredberg, Nat. Mater. **4**, 557 (2005).
[38] V. Viasnoff and F. Lequeux, Phys. Rev. Lett. **89**, 065701 (2002).
[39] J. L. Broutman and R. S. Patil, Polym. Eng. Sci. **11**, 165 (1971).
[40] D. M. Colucci, P. A. O'Connell, and G. B. McKenna, Polym. Eng. Sci. **37**, 1469 (1997).
[41] H. G. H. van Melick, L. E. Govaert, B. Raas, W. J. Nauta, and H. E. H. Meijer, Polymer **44**, 1171 (2003).
[42] D. J. Lacks and M. J. Osborne, Phys. Rev. Lett. **93**, 255501 (2004).
[43] B. A. Isner and D. J. Lacks, Phys. Rev. Lett. **96**, 025506 (2006).
[44] D. L. Malandro and D. J. Lacks, Phys. Rev. Lett. **81**, 5576 (1998).
[45] D. J. Lacks, Phys. Rev. Lett. **87**, 225502 (2001).
[46] C. Maloney and A. Lemaitre, Phys. Rev. Lett. **93**, 195501 (2004).
[47] C. E. Maloney and D. J. Lacks, Phys. Rev. E **73**, 061106 (2006).